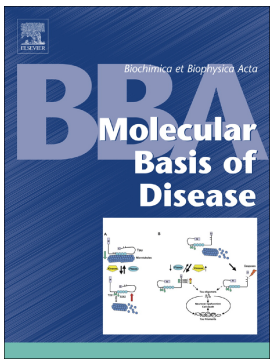


# Therapeutic targeting of telomerase ameliorates experimental choroidal neovascularization

Aman Kumar, Yosuke Nagasaka, Vinodhini Jayananthan, Asmaa Zidan, Tyler Heisler-Taylor, Jayakrishna Ambati, Shigeo Tamiya, Nagaraj Kerur

PII: S0925-4439(24)00145-5

DOI: https://doi.org/10.1016/j.bbadis.2024.167156

Reference: BBADIS 167156

To appear in: *BBA - Molecular Basis of Disease*

Received date: 19 September 2023

Revised date: 29 March 2024

Accepted date: 30 March 2024

Please cite this article as: A. Kumar, Y. Nagasaka, V. Jayananthan, et al., Therapeutic targeting of telomerase ameliorates experimental choroidal neovascularization, *BBA - Molecular Basis of Disease* (2024), https://doi.org/10.1016/j.bbadis.2024.167156

# Therapeutic targeting of telomerase ameliorates experimental choroidal neovascularization

Aman Kumar[1], Yosuke Nagasaka[2, 3], Vinodhini Jayananthan[1], Asmaa Zidan[1], Tyler Heisler-Taylor[1], Jayakrishna Ambati[2, 3], Shigeo Tamiya[1], Nagaraj Kerur[1, 2, 3, 4]*

1. Department of Ophthalmology and Visual Sciences, The Ohio State University Wexner Medical Center, Columbus, OH, USA.
2. Center for Advanced Vision Science, University of Virginia School of Medicine, Charlottesville, Virginia, USA.
3. Department of Ophthalmology, University of Virginia School of Medicine, Charlottesville, Virginia, USA.
4. Department of Microbial Infection and Immunity, The Ohio State University Wexner Medical Center, Columbus, OH, USA.

* Correspondence and requests for materials should be addressed to N.K. (nagaraj.kerur@osumc.edu).

**Summary**

Choroidal neovascularization (CNV) is the principal driver of blindness in neovascular age-related macular degeneration (nvAMD). Increased activity of telomerase, has been associated with endothelial cell proliferation, survival, migration, and invasion in the context of tumor angiogenesis. Expanding on this knowledge, we investigated the role of telomerase in the development of CNV in mouse model. We observed increased gene expression and activity of telomerase in mouse CNV. Genetic deficiency of the telomerase components, telomerase reverse transcriptase (*Tert*) and telomerase RNA component (*Terc*) suppressed laser-induced CNV in mice. Similarly, a small molecule inhibitor of TERT (BIBR 1532), and antisense oligonucleotides (ASOs) targeting *Tert* and *Terc* reduced CNV growth. Bone marrow chimera studies suggested that telomerase activity in non-bone marrow-derived cells is crucial for the development of CNV. Comparison of BIBR 1532 with VEGF neutralizing therapeutic strategy in mouse revealed a comparable level of angiosuppressive activity. However, when BIBR and anti-VEGF antibodies were administered as a combination at sub-therapeutic doses, a statistically significant suppression of CNV was observed. These findings underscore the potential benefits of combining sub-therapeutic doses of BIBR and anti-VEGF antibodies for developing newer therapeutic strategies for NV-AMD. Telomerase inhibition with BIBR 1532 suppressed induction of multiple cytokines and growth factors critical for neovascularization. In conclusion, our study identifies telomerase as a promising therapeutic target for treating neovascular disease of the eye and thus provides a proof of principle for further exploration of telomerase inhibition as a novel treatment strategy for nvAMD.

## Introduction

In neovascular age-related macular degeneration (nvAMD) abnormal blood vessel growth beneath the macula leads to retinal damage and severe vision loss. Understanding the underlying mechanisms driving ocular angiogenesis has paved the way for multiple VEGF- targeted ocular therapeutics. Although intraocular anti-VEGF therapy has had a dramatic impact on the visual outcomes of nvAMD, several challenges persist. VEGF is critical for maintenance of RPE, photoreceptors, and other retinal cells. As a result several adverse effects on multiple retinal cells have been reported in animal models (Ford et al., 2012; Kurihara et al., 2012; Nishijima et al., 2007; Takeda et al., 2009) and in patients receiving prolonged anti-VEGF therapy (Comparison of Age-related Macular Degeneration Treatments Trials Research et al., 2012; Grunwald et al., 2013; Rofagha et al., 2013). Furthermore, loss in therapeutic efficacy coupled with increased rates of macular atrophy and subretinal fibrosis are also significant risks associated with the long-term use anti-VEGF therapy (Rofagha *et al.*, 2013). Therefore, better understanding of the molecular mechanisms responsible for driving CNV are needed for the development of newer therapeutic strategies with minimal effect on homeostatic cellular functions.

Advances in cancer research have revealed that vascular tissues in human and mouse tumors express elevated levels of telomerase and that increased telomerase activity confers proangiogenic potential (Falchetti et al., 2003; Pallini et al., 2001b). In line with these observations, telomerase activity has been reported to both induce VEGF levels (Liu et al., 2016) and mediate VEGF-driven angiogenesis (Zaccagnini et al., 2005). While loss of telomerase induces senescence, telomerase hyperactivity promotes hyperproliferative phenotypes in endothelial cells (Chang and Harley, 1995; Whikehart et al., 2000; Yang et al., 1999; Yang et al., 2001). Telomerase is a ribonucleoprotein complex consisting of telomerase reverse transcriptase (TERT) and telomerase

RNA component (TERC), a non-coding RNA that serves as a template for TERT enzymatic activity (Urquidi et al., 2000). Telomerase levels in somatic cells are either very low or undetectable. Conversely, telomerase in the neovessels of cancer tissue, alike VEGF and other potent angiogenic factors (Folkman, 1971; Hanahan and Folkman, 1996), is highly upregulated (Artandi et al., 2002; Falchetti et al., 2000; Hiyama et al., 1995; Kim et al., 1994; Li et al., 2005; Pallini et al., 2001a; Sarin et al., 2005; Shay and Bacchetti, 1997; Stewart et al., 2002), thus making it an ideal therapeutic target.

Here we identify a proangiogenic role for telomerase in a mouse model of nvAMD. We show that telomerase activity is induced in CNV, and genetic and pharmacological targeting of telomerase components TERT and TERC suppress CNV. These studies identify telomerase as a promising therapeutic target for the treatment of neovascular diseases of the eye. Our studies also provide a strong foundation for further exploration of telomerase inhibition as a novel and effective therapeutic strategy for managing nvAMD and other ocular diseases driven by pathological neovascularization such as diabetic retinopathy (DR), retinopathy of prematurity (ROP), corneal neovascularization, and neovascular glaucoma.



## Results

### Telomerase expression and activity are upregulated in the laser-induced CNV mouse model

To examine the involvement of telomerase in CNV, *Tert* gene expression was analyzed in vivo. Elevated levels of *Tert* mRNA were observed in the RPE and choroid of laser-induced CNV mice compared to control mice without laser injury (Fig. 1A). To further investigate the activity level of telomerase in CNV, RPE and choroid lysates were analyzed by the Telomeric Repeat

Amplification Protocol (TRAP) assay. RPE and choroid from eyes with CNV displayed elevated levels of telomerase activity compared to these tissues from control mice (Fig. 1B). These findings collectively indicate that telomerase gene expression and activity are significantly induced in angioproliferative tissue in CNV.

**Telomerase deficiency attenuates CNV growth after laser injury**

The functional role of telomerase in CNV development was investigated by using *Tert*$^{-/-}$ and *Terc*$^{-/-}$ mice. The *Tert*$^{-/-}$ and *Terc*$^{-/-}$ mice used in our study are on 129/C57BL/6J mixed genetic background which have unusually long telomere, as results no phenotypes are observed in these mice until telomeres become critically short in late generations homozygous knockout mice (G4-G6) (Blasco et al., 1997; Hemann and Greider, 2000; Hemann et al., 2001; Lee et al., 1998). We compared CNV growth between WT and first generation (G1) *Tert*$^{-/-}$ mice generated through intercrossing of *Tert*$^{+/-}$ animals. CNV lesions were labeled with isolectin B4 and the volume of the neovascular lesion was quantified using confocal microscopy. We found that *Tert*$^{-/-}$ mice had significantly reduced CNV growth (Fig. 1C-D). Next we examined CNV in *Terc*$^{+/-}$, generation 1 (G1) and 3 (G3) *Terc*$^{-/-}$ mice. Similar to *Tert*$^{-/-}$ mice, CNV volume were significantly reduced in both G1 and G3 *Terc*$^{-/-}$ mice (Fig. 1E-F). Collectively, these findings underscore the critical role of telomerase in the process of CNV growth. Since the telomere shortening is not overserved in G1 *Tert*$^{-/-}$ and *Terc*$^{-/-}$ mice, it is likely that the reduced CNV in *Tert*$^{-/-}$ and *Terc*$^{-/-}$ mice stems from mechanisms independent of telomere length.

**Antisense oligonucleotide (ASO) therapies targeting *Tert* and *Terc* suppress laser-induced CNV in mice**

Our studies in *Tert*$^{-/-}$ and *Terc*$^{-/-}$ mice suggested a proangiogenic role of telomerase in laser-induced CNV development (Fig. 1C-F). To further confirm the role of telomerase in CNV development and to assess whether telomerase can be therapeutically targeted, we tested the effect of *Tert* and *Terc*-targeted synthetic ASOs on the development of laser-induced CNV. The ASOs effectively reduced the *Tert* and *Terc* gene expression (supplementary Fig. 1A-B). CNV volume was notably decreased in WT mice administered with intravitreous *Tert* and *Terc* targeting ASOs, compared to mice administered scrambled ASO (Fig. 2A-C). These results provide further evidence supporting the important role of telomerase in the development of CNV pathology.

**Telomerase activity in non-bone marrow-derived cells contributes to CNV development**

To determine the cellular origin of the proangiogenic activity of telomerase, we performed experiments in bone marrow chimeric mice. Laser-induced CNV volumes were not significantly different in WT mice receiving *Tert*$^{-/-}$ bone marrow (*Tert*$^{-/-}$ →WT) compared to the control group WT mice receiving WT bone marrow (WT →WT) (Fig. 3A-B; supplementary Fig. 1C). Likewise, there was no difference in CNV volumes between *Tert*$^{-/-}$ mice receiving *WT* bone marrow (WT →*Tert*$^{-/-}$ ) and *Tert*$^{-/-}$ mice receiving *Tert*$^{-/-}$ bone marrow (*Tert*$^{-/-}$→*Tert*$^{-/-}$) (Fig. 3A-B; supplementary Fig. 1C). However, as expected, *Tert*$^{-/-}$ →*Tert*$^{-/-}$ mice had a significantly low level of angiogenesis compared to WT →WT mice (Fig. 3A-B). Taken together, our observations suggest that telomerase activity in non-bone marrow-derived cells is crucial for the development of CNV.

**Pharmacological targeting of telomerase suppresses laser-induced CNV**

To assess the therapeutic potential of telomerase inhibition as an angiosuppressive strategy, we utilized BIBR 1532, a selective telomerase inhibitor (Altamura et al., 2020). Based on our observation that laser-induced CNV has elevated telomerase activity (Fig. 1B), we first confirmed the telomerase inhibitory activity of BIBR 1532 in mouse CNV. BIBR 1532 was administered via intravitreous injection in wild type mouse eyes with laser-induced CNV (Fig, 4A). Protein lysates from RPE and choroid tissues were analyzed by the TRAP assay to assess telomerase activity. As expected, intravitreous administration of BIBR 1532 in wild type mice significantly reduced telomerase activity in CNV (Fig. 4A-B). Next, we evaluated the impact of BIBR 1532 on neovascular growth in vivo. Intravitreous administration of BIBR 1532 significantly reduced laser-induced CNV (Fig. 4A, and Fig. 4C-D). Furthermore, we investigated the inhibitory effect of BIBR on CNV volume using a range of BIBR 1532 doses (166-1326 pg/eye). While there was a progressive reduction in CNV volume with increasing BIBR 1532 dose, the inhibitor effects were statistically significant at 1326 pg/eye (Fig. 4E). To determine the specificity of BIBR 1532 in reducing CNV size through a telomerase-dependent mechanism, we administrated BIBR 1532 intravitreouslly to *Tert*$^{-/-}$ mice and determined its effect on growth of CNV. No changes in CNV growth in *Tert*$^{-/-}$ mice treated with BIBR 1532 were observed, indicating that BIBR 1532 induces CNV suppression specifically through the inhibition of telomerase (Fig. 4F-G).

**Telomerase inhibition suppresses induction of angiogenic factors**

Considering the effective suppression of angiogenesis by BIBR 1532 in laser-induced CNV we further investigated the underlying molecular processes. We investigated the impact of BIBR 1532 on various angiogenic and growth factors using Luminex-based quantification. The results indicated that several of the potent angiogenic mediators (such as angiopoietin-2, MIP-1a, Endoglin, FGF-2, HGF, SDF-1, and KC) induced by laser injury were suppressed upon administration of BIBR (Supplementary Fig. 2A). We further compared the anti-angiogenic effect of BIBR 1532 with anti-VEGF neutralizing antibodies. Both treatments demonstrated comparable efficacy in significantly reducing CNV growth (Fig. 5A-B). Notably, a combination therapy utilizing sub-therapeutic doses of BIBR 1532 and anti-VEGFA antibodies yielded a statistically significant suppression of CNV, exceeding the effect of either drug alone (Fig. 5D). However, this enhanced effect was not evident when using therapeutic doses of either BIBR 1532 or anti-VEGF antibodies, indicating a potential 'floor effect' phenomenon where the efficacy of the treatment plateaus at higher doses (Fig. 5B-C). Prompted by previous studies (Liu *et al.*, 2016), we examined the effect of TERC and TERT on VEGF promoter activity by co-transfecting VEGF promoter firefly luciferase construct with TERT and TERC expression plasmids in HEK293T cells. These studies revealed that both TERC and TERT induce VEGF promoter activity, and their co-expression has a cumulative effect on this activity. (Supplementary Fig. 2B). These findings collectively suggest that the telomerase inhibitor BIBR 1532 suppresses angiogenesis potentially through VEGF-dependent and independent mechanisms, such as by suppressing other cytokines, which are involved in the proangiogenic activity of telomerase in CNV.

**BIBR 1532, does not induce morphological and histological changes in the healthy mouse eye**

Considering the potent antiangiogenic efficacy of BIBR in laser-induced CNV model, we examined if the inhibitor has any adverse effect on retinal structure. BIBR 1532 (1326pg/eye) was

administered via intravitreal injection in WT mice and retinal structure was assessed by fundus photography, spectral domain-optical coherence tomography (SD-OCT), and histology There were no observable morphological changes in the fundus (Supplementary Fig. 3A). Similarly, SD-OCT imaging showed no visible abnormalities or differences in the thickness of retinal layers between the BIBR 1532- and PBS-treated groups (Supplementary Fig. 3B-C). To further investigate any potential histological alterations, we performed haemotoxylin and eosin (H&E) staining on paraffin-embedded eye sections. Consistent with the fundus and SD-OCT findings, these histological analyses revealed no evidence of tissue abnormalities or changes in retinal layer thickness (Supplementary Fig. 3D-E).

**Discussion**

Telomerase, an enzyme responsible for maintaining telomere length, is highly expressed in numerous cancer types and reported to promote tumor angiogenesis (Falchetti *et al.*, 2003; Liu *et al.*, 2016; Pallini *et al.*, 2001a; Zaccagnini *et al.*, 2005). Telomerase inhibitors have shown promising results in cancer therapy by specifically targeting the cancer cells (Chiappori et al., 2015; Relitti et al., 2020). However, the role of telomerase in ocular neovascularization and its potential contribution to pathologies such as nvAMD have been unknown. To address this, we explored the potential involvement of telomerase in laser-induced CNV, a mouse model of nvAMD (Nowak, 2006). Although the laser-induced CNV mouse model does not fully recapitulate the entire pathological process of human CNV development, it remains a standard preclinical model for testing of nvAMD therapeutics.

Our study presents novel evidence of the involvement of telomerase in the development of CNV in a mouse model. Telomerase consists of a catalytic subunit called TERT and an essential RNA component called TERC, which serves as a template for telomeric DNA elongation (Blasiak et al., 2021; Rossiello et al., 2022). Our results demonstrate that telomerase expression and activity are upregulated in CNV tissues compared to control tissues without laser injury. The upregulation of telomerase expression and activity in CNV tissue supports the notion that telomerase plays a critical role in the development of CNV. Additionally, the functional role of telomerase in CNV was investigated using G1 *Tert*$^{-/-}$ and *Terc*$^{-/-}$ mice, which revealed a significant reduction in CNV growth in these knockout mice compared to wild-type mice. Furthermore, we explored the therapeutic potential of *Tert* and *Terc*-targeted ASOs and TERT inhibitor BIBR 1532, all of which effectively suppressed the growth of laser-induced CNV. The pharmacological targeting of telomerase using BIBR 1532 demonstrates promising therapeutic potential. The specificity of BIBR 1532 in inhibiting telomerase-dependent CNV growth is supported by the lack of its effect in *Tert*$^{-/-}$ mice, further validating its mechanism of action.

Previous research suggests that due to their inherently long telomeres, *Tert*$^{-/-}$ and *Terc*$^{-/-}$ mice exhibit normal phenotypes until telomere shortening reaches critical levels in later generations (G4-G6) (Blasco *et al.*, 1997; Hemann and Greider, 2000; Hemann *et al.*, 2001; Lee *et al.*, 1998). Therefore, our interventions targeting telomerase (i.e. G1 *Tert*$^{-/-}$ and *Terc*$^{-/-}$ mice, BIBR1532, and ASOs targeting *Tert* and *Terc*) are unlikely to induce critical telomere shortening in the timeframe of these experiments. Hence the observed reduction in the CNV likely arises from mechanisms independent of telomere length. Telomerase exhibits several extra-telomeric activities (known as non-canonical activity of TERT), with potential avenues for its proangiogenic effects. For example

hTERT has been reported to induce VEGF promoter activity via interaction with Sp1 transcription factor (Liu *et al.,* 2016). In this context, tumor implanted in G1 *Tert*$^{-/-}$ mice displayed retarded growth and VEGF expression (Liu *et al.,* 2016). Consistent with these studies, we report that both TERT and TERC augment VEGF promoter activity in a luciferase reporter system (Supplementary Fig. 1D).

Additionally, telomerase has been reported to promote NF-κB-driven gene expression (Ghosh et al., 2012), suggesting that telomerase inhibition during CNV might suppress inflammation, a critical component of angiogenesis. Another potential mechanism involves TERT's role as a modulator of the Wnt–β-catenin signaling pathway (Choi et al., 2008; Park et al., 2009). TERT, in complex with the Wnt transcription factor BRG1/SMARCA4, physically binds to Wnt-target genes, thereby promoting their expression (Choi *et al.*, 2008; Park *et al.*, 2009). Notably, several proangiogenic genes, including VEGFA, FGF, Norrin, MMP7, c-Myc, SDF-1, and endothelin-1, are direct targets of Wnt signaling. Consistent with this, FGF, endothelin-1, VEGF protein levels were reduced in BIBR 1532-administed CNV tissue (Supplementary Figure 1C). Additionally TERT has been reported to impact DNA methylation and chromatin remodeling (Masutomi et al., 2005; Young et al., 2003; Yu et al., 2018), hence it can be speculated that elevated TERT activity might induce epigenetic changes leading to altered transcriptional program in the context of angioproliferative conditions. Interestingly many of non-canonical activity of TERT such as the proliferation of hair follicle stem cells (Sarin *et al.*, 2005), the Wnt signaling (Park *et al.*, 2009), and the Myc-driven onogenesis (Koh et al., 2015) have been reported to be independent or its catalytic activity at the telomeric ends. In contrast to these reports, a tumor promoting non-canonical activity of TERT has been reported to be dependent on the expression of TERC (Cayuela et al., 2005). In our investigation, utilizing a VEGF promoter activity assay, we observed that both

TERT and TERC individually have the capacity to enhance VEGF promoter activity. interestingly, when present together, these components exhibit a synergistic effect, further augmenting VEGF promoter activity. It is conceivable that the formation of TERT-TERC complexes optimizes their conformation, potentially facilitating their efficient recruitment to the VEGF promoter or their interaction with additional factors crucial for this activity. To comprehensively understand the mechanism underlying the synergistic activity of TERT and TERC on the VEGF promoter, further studies are warranted.

Interestingly sub-therapeutic doses of BIBR 1532 and anti-VEGFA antibodies yielded a statistically significant suppression of CNV, exceeding the effect of either drug alone (Fig. 5D). However, this cooperative effect was not evident when using therapeutic doses of either BIBR 1532 or anti-VEGF antibodies, indicating a potential 'floor effect' phenomenon where the efficacy of the treatment plateaus at higher doses (Fig. 5B-C). Further research is needed to fully understand the intricate mechanisms underlying the proangiogenic activity of telomerase, as well as to comprehensively characterize the nature and mechanisms of interaction between BIBR 1532 and anti-VEGF strategies.

Our bone marrow chimera studies indicate that telomerase activity in non-bone marrow-derived cells is crucial for CNV development. These findings suggest that the proangiogenic activity of telomerase in CNV likely arises from endothelial or other stromal cells (e.g., pericytes, RPE,) in the local environment. Further research employing *Tert* or *Terc* reporter mice and conditional knockout mice is needed to precisely identify and define the contribution of various cell types. While the contribution of infiltrating myeloid cells in CNV development has been well-established by multiple studies (Andriessen et al., 2021; Iwanishi et al., 2016; Sakurai et al., 2003a; Wang et

al., 2012), our findings emphasizes the importance of telomerase activity in tissue-resident cells. Interestingly, previous studies have reported that endothelial progenitor cells (EPCs) retain a high level of telomerase activity (Ingram et al., 2004); therefore, it is possible that telomerase activity in tissue-resident EPCs plays a critical role in endothelial cell proliferation in response to angiogenic stimuli. Further studies are needed to provide a detailed understanding of the role of EPCs in development of CNV and other pathological neovascular conditions of the eye. One of the limitations of the bone marrow chimera study is that the irradiation, in addition to the hematopoietic stem cells (HSCs) in the bone marrow, can also deplete other rapidly dividing cell populations such as the tissue-resident progenitor cells. Thus the role of such tissue-resident progenitor cells cannot be ruled out.

Interestingly our study showed that BIBR 1532 suppresses laser-induced CNV with comparable efficacy to anti-VEGF neutralizing antibodies. These findings provide important insights into the role of telomerase in CNV pathology and suggest its potential as a therapeutic target for nvAMD. Although intraocular anti-VEGF therapy has had a dramatic impact on the visual outcomes of neovascular diseases of the eye, several challenges persist. Since VEGF is critical for maintenance of RPE, photoreceptors, and other retinal cells, several adverse effects on multiple retinal cells have been reported in animal models (Ford *et al.*, 2012; Kurihara *et al.*, 2012; Nishijima *et al.*, 2007; Takeda *et al.*, 2009) and in patients receiving prolonged anti-VEGF therapy (Comparison of Age-related Macular Degeneration Treatments Trials Research *et al.*, 2012; Grunwald *et al.*, 2013; Rofagha *et al.*, 2013). Furthermore, loss in therapeutic efficacy coupled with increased rates of macular atrophy and subretinal fibrosis are also significant risks associated with the long-term use anti-VEGF therapy (Rofagha *et al.*, 2013). Therefore, telomerase presents a potentially

attractive alternative for treating neovascular diseases of the eye. One advantage of targeting telomerase for nvAMD is its minimal expression in non-proliferating somatic cells, which we predict would minimize off-target effects of the inhibitor. Whether telomerase inhibition will suffer challenges similar to those from anti-VEGF therapy remains to be elucidated in future studies. Short-term telomerase inhibition (7 days) with BIBR 1532 showed no apparent abnormalities in retinal imaging studies (Supplementary Figure 3). However, before further exploration of telomerase targeted therapies, it is crucial to thoroughly investigate the potential adverse effects of long-term telomerase inhibition in the eye. Another challenge with the pharmacological targeting telomerase include need for development of a method for sustained intraocular delivery of inhibitors for a chronic condition like AMD.

In conclusion, our study provides compelling evidence that telomerase plays a critical role in the development of experimental choroidal neovascularization. The findings of our study suggest that telomerase inhibition could be a potential therapeutic target for nvAMD. However, further studies employing additional models are needed to investigate the long-term safety and efficacy of telomerase inhibition in the eye.



## Materials and Methods

### Animals

Male and female C57BL/6J, *Tert*$^{-/-}$ and *Terc*$^{-/-}$ mice aged between 8 to 12 weeks were used in this study. C57BL/6J, *Tert*$^{-/-}$ and *Terc*$^{-/-}$ mice were obtained from the Jackson laboratory. *Tert*$^{+/-}$ (Strain #:004132, JAX) and *Terc*$^{+/-}$ (Strain #:005423, JAX) mice were bred as heterozygotes, and resulting generation 1 (G1) homozygous knockout and wildtype litter mates were used for

experiments. All experimental procedures were approved by the Institutional Animal Care and Use Committee of The Ohio State University and/or University of Virginia. Studies were conducted in accordance with the principles outlined in the Association for Research in Vision and Ophthalmology (ARVO) Statement for Use of Animals in Ophthalmic and Vision Research. The mice were housed in a standard sterile facility with ventilated cage systems. The environment maintained a controlled temperature and humidity, with a 12-hour light and 12-hour dark cycle. The animals had access to sterilized, irradiated rodent diet (a standard laboratory mouse diet) ad libitum and received sterile water through automatic water systems. For all the procedures, the mice were anesthetized by intraperitoneal injection of avertin (500µg/g of body weight).

**Antisense oligonucleotides**

In vivo ready ASOs, Antisense LNA GapmeR targeting mouse *Tert*, and *Terc* genes or scramble were purchased from Qiagen (Cat# 339523). The ASO sequence information is provided in the supplementary table 1.

**Cell culture and treatments**

RAW 264.7 cells (ATCC, #TIB-71) were cultured in Dulbecco's modified Eagle's medium (DMEM; Thermofisher, #12430062) supplemented with 10% fetal bovine serum (FBS) and 1% penicillin–streptomycin. The cells were maintained at 37$^{o}$C with 5% $CO_2$ in a suitable incubator. Prior to transfection, the cells were seeded in a 12-well plate and allowed to reach approximately 70% confluency. The cells were transfected with 0.5µg of *Tert/Terc* (ASOs) along with Scrambled

ASO (synthesized by Qiagen) using Lipofectamine 3000 (Thermofisher, #L3000001) for 48 hours, as described previously (Banerjee et al., 2021).

**Luciferase promoter activity assay:** HEK293T cells cultured in 12- well plate were used to assess VEGF promoter activity using luciferase reporter system. VEGF promoter Firefly luciferase construct (300ng) (Addgene, Plasmid #66128) was co-transfected with an empty vector, TERC (300ng) (Abmgood Cat# 46496061), or TERT (300) (Addgene Plasmid #51631) expression plasmids alone or in combination. Renilla reporter plasmid (50ng) under HSV-thymidine kinase promoter (Promega Cat# E2241) was also transfected and was used for normalization. Cells were transfected at 50-60% confluence using Lipofectamine 3000 reagent (Invitrogen, cat# L3000001); experimental design ensured each well received equal amount of total plasmid DNA. 40 hours post transfection, cells were lysed and Firefly and Renilla luciferase activity were measured sequentially using Dual-Luciferase® Reporter Assay System (Promega, Cat# E1910) following manufacture's protocol.



**Laser-induced choroidal neovascularization mouse model**

Laser photocoagulation was performed using either slit lamp delivery system or Phoenix MICRON® Image-Guided Laser System. Using slit lamp delivery system laser photocoagulation (532 nm, 200 mW, 100 ms, 75 μm; Iridex, Mountain View, CA) was performed as previously described (Kleinman et al., 2008; Nozaki et al., 2006; Sakurai et al., 2003b).

The laser photocoagulation using the Micron IV phoenix image-guided laser system was performed following a previously established procedure (Gong et al., 2015). This system utilizes Meridian Merilas 532 green laser photocoagulator. Laser photocoagulations lesions were induced with spot diameter of 50μm, delivering a 70ms pulse of 220mW power. Prior to each experiment, the laser system was calibrated to ensure accurate power output. To facilitates the procedure, the mice eyes were dilated using tropicamide and phenylephrine drops, and a general eye lubricant was applied to the cornea. Once the pupils were dilated, the mice were positioned to visualize fundus on a computer screen connected to the micron system, and the laser beam was directed onto the fundus. Four laser burns were created around the optic disc at the 3, 6, 9, and 12 o'clock positions, approximately 2–3 optic disc diameter away from the optic nerve. Confirmation of the Bruch's membrane rupture was observed by the formation of a bubble at the center of the laser spot. CNV lesions with hemorrhagic complications were included in the study.

**Flat mount staining and CNV volume measurement**

On day 7 after laser photocoagulation, all mice were sacrificed, and eyes were carefully removed using curved forceps and immediately fixed in 4% paraformaldehyde (PFA) for 1 hour at room temperature. Under a dissecting microscope, the anterior part of the eye, including the cornea and lens, was dissected away using spring scissors. The whole neural retina was then gently removed, leaving behind the posterior cup consisting of the RPE, choroid and sclera. The posterior eye cups were subsequently washed with PBS and dehydrated followed by rehydration by immersing the tissue in increasing and decreasing concentrations of methanol solution (75%, 50% and 25%). Afterwards, posterior eye cups were washed twice with phosphate-buffered saline (PBS) and then blocked using a solution containing 1% goat serum and 0.5% Triton X-100 for 1 hour at room

temperature. To stain the CNV lesions, the eye cups were incubated overnight at 4ºC with FITC-labeled Griffonia Simplicifolia Lectin I (GSL1) Isolectin B4 (0.7%, Vector laboratory, #FL-1201). Afterward, the eye cups were washed with 0.1% Triton X-100 in PBS. To prepare flat mounts, the posterior eye cups were carefully flattened onto glass slides by making 4 radial cuts, ensuring that the sclera faced downwards. The flat mounts were then mounted with an antifade mounting medium (Vector laboratory, #H-1400). The Isolectin B4-stained CNV lesion were imaged using a Nikon A1R or AXR confocal microscope, and fluorescence images of the CNV lesions were captured using consistent laser power and gain settings to minimize instrumental variability across lesions. The 3D volume of the CNV lesions was calculated using Nikon NIS-Elements software, or as described previously using ImageJ (Bogdanovich et al., 2016; Yasuma et al., 2016).

**Intravitreal injections.**

For intravitreal injections, the ASOs and antibodies were dissolved in PBS. BIBR 1532 stock solutions was prepared in dimethyl sulfoxide (DMSO) and diluted in PBS before injection. 1µl (1µg) ASO in PBS, was administrated twice; the first injection occurred 3 days before the laser photocoagulation (days -3), and the second injection took place 3 days after the laser treatment ( day 3). Similarly, 1µl of BIBR 1532 was administered to deliver the compound at 166-1326 pico gram/eyes. BIBR 1532 was injected twice into the vitreous of the eye. The first dose was administrated on day 1 before (day -1) the laser treatment, and the second dose was given after 3 days (day 3) of laser photocoagulation. Equivalent amount of DMSO diluted in PBS was used as the vehicle for these injections. Furthermore, 1µl of anti-VEGF (2, 5, or 10ng; R&D Systems, #AF-493), or IgG (2, 5, or 10ng; ThermoFisher, #02-6202) were delivered once immediately after

the laser treatment. All intravitreal injections were performed on anesthetized mice under a surgical microscope using a 33-gauge needle fitted in a Hamilton syringe.

**Real-Time Polymerase Chain Reaction**

To examine gene expression in RPE/choroid, tissues were harvested three days post-laser injury. Tissues from both eyes of a mouse were combined to generate one pooled sample per mouse. The total RNA was extracted using RNeasy Mini Kit (Qiagen #74104) following the manufacturer's instructions. Subsequently, cDNA synthesis was performed using the QuantiTect Rev. Transcription Kit (Qiagen, #205311) according to the manufacturer's protocol. The resulting cDNA samples were stored at −20°C till further analysis**.** Real-time polymerase chain reaction (RT-PCR) was conducted using SYBR green master mix on an Applied Biosystems QuantStudio$^{TM}$ 3 machine. The reference gene for normalization was 18s rRNA. The relative gene expression of *Tert* was determined using the ΔΔCt method. Primer sequences utilized for gene expression analysis can be found in Supplementary Table 1.

**Telomerase Activity**

Telomerase activity in RPE/choroid tissue was assessed using TeloTAGGG Telomerase PCR ELISA$^{PLUS}$ kit, following the manufacturer's instructions (Sigma Aldrich, #12013789001). The RPE/choroid tissues collected at 7 days post laser injury were lysed in 200µl of lysis buffer and incubated on ice for 2 hours. The lysates were then centrifuged, and the supernatant was carefully transferred to new 1.5ml tubes. The protein content in the samples was estimated using a bicinchoninic acid (BCA) assay following the kit protocol (Fisher scientific, #P123225). Negative

controls were prepared by treating the tissue extract with RNase. The TRAP reaction was performed using 3µg of total protein in a thermocycler, employing the P1-TS1 primer and anchor primer P2 to generate telomerase-specific products with 6 nucleotide increments. An internal standard product of 216 bp was included. After PCR amplification, the products were split into 2 aliquots. Each aliquot was denatured and hybridized separately to digoxigenin-labeled detection probes specific for telomeric repeats and the Internal Standard (IS), incubating at 37$^{o}$C for 2 hours. The resulting products were immobilized to a streptavidin-coated microplate via the biotin-labeled primer. Finally, they were detected using an antibody against digoxigenin conjugated to horseradish peroxidase. Color development was achieved by adding the TMB substrate, and absorbance was measured at 450 nm (with a reference wavelength of approximately 690 nm) using a microtiter plate (ELISA) reader within 30 minutes after adding the stop reagent. The absorbance values were reported as A450 nm – A690 nm. To calculate the relative telomerase activity, the following formula was used: RTA = [(absorbance of sample – absorbance of negative control)/(absorbance of internal control (IS) of sample)]/ [(absorbance of control template – absorbance of lysis buffer)/absorbance of IS of control template] X 100.



**Histology**

Eyes were fixed in 4% paraformaldehyde (PFA) and processed for paraffin embedding. 10µm thick serial sections were stained with H&E and imaged using a slide scanning microscope (Olympus VS200). The thickness of retinal layers was measured using Nikon NIS elements software.

**Spectral-domain Optical coherence tomography (SD-OCT)**

OCT was conducted on mice 7 days after the administration of BIBR (1326 pg/eye) or vehicle injections. The mice were anesthetized, and their pupils were dilated using tropicamide and phenylephrine drops. SD-OCT imaging was performed using the Envisu R2200 VHR system and InVivoVue software. Linear scan, radial scan, and rectangular scan were obtained for each eye. The acquired scans were averaged suing the InVivoVue reader and subsequently analyzed in InVivoVue Diver.

**Quantification of cytokines**

Multiple cytokines, chemokines, and growth factors in mouse RPE/choroid samples were simultaneously analyzed using the Luminex™ 200 system (Luminex, Austin, TX, USA). Eve Technologies' Mouse Angiogenesis & Growth Factor 16-Plex Discovery Assay® service was utilized to perform these analyses. The assay included markers such as Amphiregulin, Angiopoietin-2, EGF, Endoglin, Endothelin-1, Fas Ligand, FGF-2, Follistatin, G-CSF, HGF, IL-1β, IL-6, IL-17, KC, Leptin, MCP-1, MIP-1α, PLGF-2, Prolactin, sALK-1, SDF-1, TNFα, VEGF-A, VEGF-C, and VEGF-D. Sensitivities of these markers in the assay ranged from 0.2 to 50.3 pg/mL.

**Bone marrow transplantation.**

8-12 weeks old recipient mice were identified and offered antibiotic containing drinking water (Neomycicn sulfate 2mg/ml) 3 days prior to planned irradiation day. Recipient mice were prepared

by exposing them to a total dose of 13 Gy X ray irradiation (RS-2000 Biological System, Rad Source Technologies inc.) delivered in two equal fractions (6.5 Gy) with a 3-hour interval. Donor bone marrow cells were isolated from the femoral and tibial bones and resuspended DMEM medium at a concentration of $2.5 \times 10^7$ cells/ml. Donor bone marrow cells ($5 \times 10^6$ in 200µl) were injected in recipient mice (24 hr post irradiation) via tail vein. The transplanted bone marrow cells were allowed to reconstitute in the recipient mice for 45-60 days. Engraftment of the donor cells in the recipient mice was assessed by PCR-based genotyping of DNA purified from peripheral blood.

**Statistical analysis**

Statistical analyses were conducted using GraphPad Prism software (version 9.0, GraphPad Software Inc., CA, USA). The normality of the data distribution was assessed using the D'Agostino and Pearson omnibus normality tests. For comparing differences between the two groups, unpaired t-tests or Mann-Whitney tests were utilized depending on the normality of the data. One-way or two-way ANOVA or Kruskal Wallis tests were employed for comparing difference among more than two groups. Statistical significance was defined as a P-value less than 0.05. Illustrations in Fig. 2A, Fig. 4A, and Fig. 5A were created with BioRender.

**Author contributions:**

A.K., Y.N., V.J., A.Z., T.T., and S.T., performed experiments, analyzed data, and/or edited the manuscript. J.A., analyzed data and edited the manuscript. A.K. and N.K., wrote the manuscript

and prepared the figures. N.K., conceived and directed the project. All authors had the opportunity to discuss the results and comment on the manuscript.

**Acknowledgements:**

We thank Daniel Biddle, Kara Paulk, and Eileen Sanz (The Ohio State University) technical assistance. We thank Bradley D. Gelfand (University of Virginia) for insightful discussions. We thank the Ohio State University Vision Sciences Research Core Program (OSU-VSRCP) under P30EY032857 for assisting with ophthalmic imaging and confocal microscopy. This project was supported by grants to N.K. from NIH (R21EY030651, R01AI14874, and R01AI14874-03S1) and Ohio Lions Eye Research Foundation (OLERF). This work was supported in part by Research to Prevent Blindness (RPB) New Chair Challenge Grant. J.A., was supported by NIH grants (R01EY024068, R01EY028027, R01EY029799, and R01EY031039). S.T., was supported by grants from the NIH (R01EY030060) and OLERF.

**Conflict of Interest Disclosures:**

N.K. is named as an inventor on a patent application on non-canonical signaling activity of cGAMP filed by the University of Virginia. N.K. and J.A., are named as inventors on patent applications on macular degeneration filed by the University of Virginia or the University of Kentucky. J.A., is a co-founder of DiceRx, iVeena Holdings, iVeena Delivery Systems and Inflammasome Therapeutics, and, unrelated to this work, he has been a consultant for Abbvie/Allergan, Boehringer-Ingelheim, Janssen, Olix Pharmaceuticals, Retinal Solutions, and Saksin LifeSciences. The other authors declare no competing interests.

**Data availability**

Data will be made available on request

**Ethics statement**

All experimental procedures were approved by the Institutional Animal Care and Use Committee of The Ohio State University (2021A00000041) and/or University of Virginia. Studies (4151-12-19) were conducted in accordance with the principles outlined in the Association for Research in Vision and Ophthalmology (ARVO) Statement for Use of Animals in Ophthalmic and Vision Research.

**Figure legends:**

**Figure 1. Telomerase promotes laser induced CNV**. A) *Tert* mRNA levels in RPE/choroid tissue from control or laser-induced CNV mice 3 days post laser photocoagulation (n = 7 samples) are presented. B) Quantification of the telomerase activity in RPE/choroid tissue from control or laser-induced CNV mice 7 days post laser photocoagulation (n = 3 samples) is presented. C) Representative images of FITC-isolectin B4 stained CNV lesions in RPE/choroid/scleral flat mounts from wild-type (WT) mice and *Tert* knock-out mice (*Tert*$^{-/-}$) mice after day 7 of laser injury are presented. D) The confocal images of the CNV lesions from WT and *Tert*$^{-/-}$ mice were quantified using Nikon analysis software. Relative volumes of the CNV lesions are presented (n = 23 CNV lesions for WT, and 21 CNV lesions for *Tert*$^{-/-}$). E) Representative images of the FITC-isolectin B4 stained CNV lesions in *WT* mice and *Terc*$^{-/-}$ mice 7 days post-laser photocoagulation. F) The confocal images of the CNV lesions from WT and *Terc*$^{-/-}$ mice were quantified using ImageJ software. Relative volumes of the CNV lesions are presented (n = 32 CNV lesions for WT,

and 28 CNV lesions for *Terc*$^{-/-}$). Data are presented means ± SEM. P-values are obtained by Mann-Whitney in (A), (D) and (F) and unpaired t-test in (B). A p-value of <0.05 was considered statistically significant. (*P<0.05). Scale bar, 100µm.

**Figure 2. *Tert* and *Terc* specific antisense oligonucleotides (ASOs) suppress CNV growth**. A) Schematic representation of the ASO treatment in laser-induced CNV mouse model. B) Representative confocal images of FITC- isolectin B4 stained RPE/choroid/scleral flatmount showing CNV lesion (7 day lost laser injury) in mice administered with control (Ctr), *Tert* and *Terc* ASOs. Scale bar, 100µm. C) Quantification of CNV volume using Image J is presented (n = 40 CNV lesions for Ctr, 25 CNV lesions for *Tert* ASO, 27 CNV lesions for *Terc* ASO). Data are mean ± SEM. Statistical analysis was performed using one-way analysis of variance (ANOVA). A P-value of less than 0.05 indicates statistical significance (*P < 0.05, ns = not significant).

**Figure 3. Telomerase activity in non-bone marrow derived cells contributes to the CNV growth** A) Recipient *WT* and *Tert*$^{-/-}$ mice were transplanted with bone marrow cells derived from either from WT and *Tert*$^{-/-}$ mice. The laser-induced CNV was produced in bone marrow chimera mice 45 days post bone marrow transplantation. Representative confocal image of isolectin B4 stained CNV lesions are presented. Scale bar, 100µm. B) Quantification of CNV lesion volume using Nikon analysis software (n = 38 CNV lesions for WT>WT (R), 28 CNV lesions for *Tert*$^{-/-}$>WT (R), 37 CNV lesions for *Tert*$^{-/-}$>*Tert*$^{-/-}$ (R), 26 CNV lesions for WT> *Tert*$^{-/-}$ (R)) is presented. Where (R) represents the recipient mouse. Data are represented as mean ± SEM. P-values were obtained using Kruskal Wallis test with Dunn's correction. (*P<0.05, ns=not significant).

**Figure 4. Effect of telomerase inhibitor BIBR 1532 on laser induced CNV in mice.** A) Schematic representation of the BIBR 1532 treatment timeline. B) Telomerase activity in RPE/choroid tissue as determined by TRAP assay at day 7 after laser injury with or without BIBR 1532 (1326pg/eye) is presented (n = 4 samples each group). C) Representative images of the isolecton B4 stained CNV lesions in RPE/choroid/scleral flat mounts (at 7 days post laser injury) after intravitreal vehicle or BIBR 1532 (1326pg/eye) administration. Scale bar, 100μm. (n = 24 CNV lesions for Control, 19 CNV lesions for BIBR 1532). D) Confocal images of the CNV lesions from mice intravitreally administered with vehicle or BIBR 1532 were quantified using ImageJ. Relative CNV lesion volumes are presented. E) Dose-dependent effect of intravitreal BIBR 1532 administration was assessed by quantifying the confocal images of the CNV lesions via ImageJ analysis. Relative CNV lesion volumes are presented (n = 39 lesions for vehicle control, 35 lesions for 166pg BIBR 1532, 37 lesions 331pg BIBR 1532, 43 lesions for 663pg BIBR 1532, and 33 lesions for 1326pg BIBR 1532). F) Representative confocal images of laser-induced CNV lesions are presented from *Tert*$^{-/-}$ mice intravitreally administered with BIBR 1532 (1326pg/eye). The images were captured at day 7 post laser. Scale bar, 100μm. G) Quantification of laser-induced CNV lesions from *Tert*$^{-/-}$ mice intravitreally administered with BIBR 1532 (1326pg/eye) or vehicle is presented. The images were analyzed using Nikon Elements analysis software. Relative CNV volumes are presented (n = 16 CNV lesions for vehicle, 19 CNV lesions for 1326pg BIBR). Data are mean ± SEM. Statistical analysis was performed using unpaired t-test for (B), (D), (G) and Kruskal-Wallis with Dunn's correction for (E). A P-value of less than 0.05 indicates statistical significance (*P<0.05, ns = not significant).

**Figure 5. BIBR 1532 action is similar to Anti-VEGF therapy in inhibiting CNV growth.** A) Schematic representation of the BIBR 1532 and ant-VEGF treatment timeline. B-D)

Quantification of the laser induced- CNV lesions from mice following intravitreal administration of indicated doses of BIBR 1532 and anti-VEGF antibodies alone or in combination is presented. CNV lesion images were analyzed by Nikon Elements software. Relative CNV volumes are presented. Data are represented as mean ± SEM. Statistical analysis was performed using one-way analysis of variance (ANOVA). A P-value of less than 0.05 indicates statistical significance (*P<0.05, ns = not significant).

**Supplementary figure 1. BIBR 1532 is mediating the repression of angiogenic factors which are induced upon CNV**.

A-B) Efficiency of *Tert* and *Terc* ASOs was determined in cell culture. RAW 264.7 cells were transfected with the ASOs and transcript levels *Tert* and *Terc* were assessed by qPCR. Relative transcripts abundance is presented (n = 4 cell culture replicates each group). Data are mean ± SEM. P-values were obtained using unpaired t-test. A P-value of less than 0.05 indicates statistical significance (*P<0.05). (C) PCR-based genotyping analysis of DNA purified from the peripheral blood from the recipient mice in bone marrow chimera experiment. Blood DNA from *Tert*$^{-/-}$ recipient mice transplanted with WT bone marrow cells [WT (D) Tert (R)] show predominantly WT alleles (Lane 2 and 3). Similarly, [Tert (D) WT (R)], show predominantly *Tert*$^{-/-}$ allele (lane 4 and 5)

**Supplementary figure 2. Effect of BIBR 1532 on angiogenic factors in CNV**

A) Heat map demonstrating the relative abundance of angiogenic factors in RPE/choroid of laser-induced CNV mice with or without intravitreal BIBR1532 administration. Protein lysates at 7 day

post laser injury were analyzed by Luminex multiplex assay. Numerical value within each cell of the heatmap represents change in the cytokine level are presented (n = 4 tissue lysates sample each group). B) VEGF promoter activity was measured using ual-Luciferase® Reporter Assay System in HEK 293T cells transfected with indicated plasmids (+). Ratio of Firefly/Renilla luciferase activity are presented in the bargraph. Data are represented as mean ± SEM. Statistical analysis was performed using one-way analysis of variance (ANOVA). A P-value of less than 0.05 indicates statistical significance (*P<0.05, ns = not significant).

**Supplementary figure 3. Effect of BIBR 1532 on the retinal health.** A) Representative fundus examination of mice injected with BIBR 1532 (1326pg) or vehicle after 7 days post laser treatment (n = 6 eyes each group). B) Representative spectral-domain optical coherence tomography (SD-OCT) images of the BIBR 1532 (1326pg) or vehicle injected eyes 7 days post laser injury (n = 6 eyes each group). C) The retinal layers thickness was calculated using InVivoVue Diver software (RPE, ONL and INL) (n = 4 eyes each group). ) Histological analysis of retinal morphology using H&E staining on paraffin embedded sections of control and BIBR 1532 (1326pg) -treated eyes at 7days post laser injury. Scale bar, 50µm. E) H&E stained images were analyzed using Nikon Elements software to determine thickness of retinal layers (GCL, INL and ONL) (n = 3 eyes each group). Values are mean ± SEM. Statistical analysis was performed using 2-way ANOVA. A P-value of less than 0.05 indicates statistical significance (ns = not-significant).

| **Supplementary Table 1** | | |
|---|---|---|
| **Primers, Antisense Oligo sequence information** | **Source** | **Catalog #** |
| Ctr ASO: A*A*C*A*C*G*T*C*T*A*T*A*C*G*C | Qiagen | Antisense LNA GapmeRs Cat# 339523 |

| | | |
|---|---|---|
| *Terc* ASO:<br>G*C*T*A*A*T*G*A*A*A*A*T*C*A*G*G | Qiagen | Antisense LNA GapmeRs<br>Cat# 339523 |
| Tert ASO:<br>T*G*G*T*T*A*C*T*G*T*C*A*A*A*C*G | Qiagen | Antisense LNA GapmeRs<br>Cat# 339523 |
| qPCR mTERT Forward:<br>CTC TCT GCT GCG CAG CCG ATA C | IDT | NA |
| qPCR mTERT Reverse:<br>CCT CGT TAA GCA GCT CAA AG | IDT | NA |
| qPCR m18s rRNA Forward:<br>TTC GTA TTG CGC CGC TAG A | IDT | NA |
| qPCR m18s rRNA Reverse:<br>CTT TCG CTC TGG TCC GTC TT | IDT | NA |
| The phosphorothioate backbone modifications is indicated by "*". | | |

## References


Altamura, G., Degli Uberti, B., Galiero, G., De Luca, G., Power, K., Licenziato, L., Maiolino, P., and Borzacchiello, G. (2020). The Small Molecule BIBR1532 Exerts Potential Anti-cancer Activities in Preclinical Models of Feline Oral Squamous Cell Carcinoma Through Inhibition of Telomerase Activity and Down-Regulation of TERT. Front Vet Sci *7*, 620776. 10.3389/fvets.2020.620776.

Andriessen, E.M.M.A., Binet, F., Fournier, F., Hata, M., Dejda, A., Mawambo, G., Crespo-Garcia, S., Pilon, F., Buscarlet, M., Beauchemin, K., et al. (2021). Myeloid-resident neuropilin-1 promotes choroidal neovascularization while mitigating inflammation. EMBO Molecular Medicine *13*, e11754. https://doi.org/10.15252/emmm.201911754.

Artandi, S.E., Alson, S., Tietze, M.K., Sharpless, N.E., Ye, S., Greenberg, R.A., Castrillon, D.H., Horner, J.W., Weiler, S.R., Carrasco, R.D., and DePinho, R.A. (2002). Constitutive telomerase expression promotes mammary carcinomas in aging mice. Proc Natl Acad Sci U S A *99*, 8191-8196. 10.1073/pnas.112515399.

Banerjee, D., Langberg, K., Abbas, S., Odermatt, E., Yerramothu, P., Volaric, M., Reidenbach, M.A., Krentz, K.J., Rubinstein, C.D., Brautigan, D.L., et al. (2021). A non-canonical, interferon-independent signaling activity of cGAMP triggers DNA damage response signaling. Nat Commun *12*, 6207. 10.1038/s41467-021-26240-9.

Blasco, M.A., Lee, H.-W., Hande, M.P., Samper, E., Lansdorp, P.M., DePinho, R.A., and Greider, C.W. (1997). Telomere shortening and tumor formation by mouse cells lacking telomerase RNA. Cell *91*, 25-34.

Blasiak, J., Szczepanska, J., Fila, M., Pawlowska, E., and Kaarniranta, K. (2021). Potential of Telomerase in Age-Related Macular Degeneration-Involvement of Senescence, DNA Damage Response and Autophagy and a Key Role of PGC-1alpha. Int J Mol Sci *22*. 10.3390/ijms22137194.

Bogdanovich, S., Kim, Y., Mizutani, T., Yasuma, R., Tudisco, L., Cicatiello, V., Bastos-Carvalho, A., Kerur, N., Hirano, Y., Baffi, J.Z., et al. (2016). Human IgG1 antibodies suppress angiogenesis in a target-independent manner. Signal Transduction and Targeted Therapy *1*, 15001. 10.1038/sigtrans.2015.1.

Cayuela, M.L., Flores, J.M., and Blasco, M.A. (2005). The telomerase RNA component Terc is required for the tumour-promoting effects of Tert overexpression. EMBO reports *6*, 268-274. https://doi.org/10.1038/sj.embor.7400359.

Chang, E., and Harley, C.B. (1995). Telomere length and replicative aging in human vascular tissues. Proc Natl Acad Sci U S A *92*, 11190-11194.

Chiappori, A.A., Kolevska, T., Spigel, D.R., Hager, S., Rarick, M., Gadgeel, S., Blais, N., Von Pawel, J., Hart, L., Reck, M., et al. (2015). A randomized phase II study of the telomerase inhibitor imetelstat as maintenance therapy for advanced non-small-cell lung cancer. Ann Oncol *26*, 354-362. 10.1093/annonc/mdu550.

Choi, J., Southworth, L.K., Sarin, K.Y., Venteicher, A.S., Ma, W., Chang, W., Cheung, P., Jun, S., Artandi, M.K., Shah, N., et al. (2008). TERT promotes epithelial proliferation through transcriptional control of a Myc- and Wnt-related developmental program. PLoS Genet *4*, e10. 10.1371/journal.pgen.0040010.

Comparison of Age-related Macular Degeneration Treatments Trials Research, G., Martin, D.F., Maguire, M.G., Fine, S.L., Ying, G.S., Jaffe, G.J., Grunwald, J.E., Toth, C., Redford, M., and Ferris, F.L., 3rd (2012). Ranibizumab and bevacizumab for treatment of neovascular age-related macular degeneration: two-year results. Ophthalmology *119*, 1388-1398. 10.1016/j.ophtha.2012.03.053.

Falchetti, M.L., Pallini, R., D'Ambrosio, E., Pierconti, F., Martini, M., Cimino-Reale, G., Verna, R., Maira, G., and Larocca, L.M. (2000). In situ detection of telomerase catalytic subunit mRNA in glioblastoma multiforme. Int J Cancer *88*, 895-901.

Falchetti, M.L., Pierconti, F., Casalbore, P., Maggiano, N., Levi, A., Larocca, L.M., and Pallini, R. (2003). Glioblastoma induces vascular endothelial cells to express telomerase in vitro. Cancer Res *63*, 3750-3754.

Folkman, J. (1971). Tumor Angiogenesis: Therapeutic Implications. New England Journal of Medicine *285*, 1182-1186. 10.1056/nejm197111182852108.
Ford, K.M., Saint-Geniez, M., Walshe, T.E., and D'Amore, P.A. (2012). Expression and role of VEGF--a in the ciliary body. Invest Ophthalmol Vis Sci *53*, 7520-7527. 10.1167/iovs.12-10098.
Ghosh, A., Saginc, G., Leow, S.C., Khattar, E., Shin, E.M., Yan, T.D., Wong, M., Zhang, Z., Li, G., Sung, W.-K., et al. (2012). Telomerase directly regulates NF-κB-dependent transcription. Nature Cell Biology *14*, 1270-1281. 10.1038/ncb2621.
Gong, Y., Li, J., Sun, Y., Fu, Z., Liu, C.H., Evans, L., Tian, K., Saba, N., Fredrick, T., Morss, P., et al. (2015). Optimization of an Image-Guided Laser-Induced Choroidal Neovascularization Model in Mice. PLoS One *10*, e0132643. 10.1371/journal.pone.0132643.
Grunwald, J.E., Daniel, E., Huang, J., Ying, G.S., Maguire, M.G., Toth, C.A., Jaffe, G.J., Fine, S.L., Blodi, B., Klein, M.L., et al. (2013). Risk of Geographic Atrophy in the Comparison of Age-related Macular Degeneration Treatments Trials. Ophthalmology. 10.1016/j.ophtha.2013.08.015.
Hanahan, D., and Folkman, J. (1996). Patterns and emerging mechanisms of the angiogenic switch during tumorigenesis. Cell *86*, 353-364.
Hemann, M.T., and Greider, C.W. (2000). Wild-derived inbred mouse strains have short telomeres. Nucleic Acids Research *28*, 4474-4478. 10.1093/nar/28.22.4474.
Hemann, M.T., Strong, M.A., Hao, L.-Y., and Greider, C.W. (2001). The Shortest Telomere, Not Average Telomere Length, Is Critical for Cell Viability and Chromosome Stability. Cell *107*, 67-77. https://doi.org/10.1016/S0092-8674(01)00504-9.
Hiyama, E., Yokoyama, T., Tatsumoto, N., Hiyama, K., Imamura, Y., Murakami, Y., Kodama, T., Piatyszek, M.A., Shay, J.W., and Matsuura, Y. (1995). Telomerase Activity in Gastric Cancer. Cancer Research *55*, 3258-3262.
Ingram, D.A., Mead, L.E., Tanaka, H., Meade, V., Fenoglio, A., Mortell, K., Pollok, K., Ferkowicz, M.J., Gilley, D., and Yoder, M.C. (2004). Identification of a novel hierarchy of endothelial progenitor cells using human peripheral and umbilical cord blood. Blood *104*, 2752-2760. 10.1182/blood-2004-04-1396.
Iwanishi, H., Fujita, N., Tomoyose, K., Okada, Y., Yamanaka, O., Flanders, K.C., and Saika, S. (2016). Inhibition of development of laser-induced choroidal neovascularization with suppression of infiltration of macrophages in Smad3-null mice. Laboratory Investigation *96*, 641-651. 10.1038/labinvest.2016.30.
Kim, N.W., Piatyszek, M.A., Prowse, K.R., Harley, C.B., West, M.D., Ho, P.L., Coviello, G.M., Wright, W.E., Weinrich, S.L., and Shay, J.W. (1994). Specific association of human telomerase activity with immortal cells and cancer. Science *266*, 2011-2015.
Kleinman, M.E., Yamada, K., Takeda, A., Chandrasekaran, V., Nozaki, M., Baffi, J.Z., Albuquerque, R.J., Yamasaki, S., Itaya, M., Pan, Y., et al. (2008). Sequence- and target-independent angiogenesis suppression by siRNA via TLR3. Nature *452*, 591-597. 10.1038/nature06765.
Koh, C.M., Khattar, E., Leow, S.C., Liu, C.Y., Muller, J., Ang, W.X., Li, Y., Franzoso, G., Li, S., Guccione, E., and Tergaonkar, V. (2015). Telomerase regulates MYC-driven oncogenesis independent of its reverse transcriptase activity. The Journal of clinical investigation *125*, 2109-2122. 10.1172/JCI79134.
Kurihara, T., Westenskow, P.D., Bravo, S., Aguilar, E., and Friedlander, M. (2012). Targeted deletion of Vegfa in adult mice induces vision loss. The Journal of clinical investigation *122*, 4213-4217. 10.1172/JCI65157.
Lee, H.-W., Blasco, M.A., Gottlieb, G.J., Horner, J.W., Greider, C.W., and DePinho, R.A. (1998). Essential role of mouse telomerase in highly proliferative organs. Nature *392*, 569-574. 10.1038/33345.
Li, S., Crothers, J., Haqq, C.M., and Blackburn, E.H. (2005). Cellular and gene expression responses involved in the rapid growth inhibition of human cancer cells by RNA interference-mediated depletion of telomerase RNA. J Biol Chem *280*, 23709-23717. 10.1074/jbc.M502782200.

Liu, N., Ding, D., Hao, W., Yang, F., Wu, X., Wang, M., Xu, X., Ju, Z., Liu, J.P., Song, Z., et al. (2016). hTERT promotes tumor angiogenesis by activating VEGF via interactions with the Sp1 transcription factor. Nucleic Acids Res *44*, 8693-8703. 10.1093/nar/gkw549.

Masutomi, K., Possemato, R., Wong, J.M., Currier, J.L., Tothova, Z., Manola, J.B., Ganesan, S., Lansdorp, P.M., Collins, K., and Hahn, W.C. (2005). The telomerase reverse transcriptase regulates chromatin state and DNA damage responses. Proceedings of the national academy of sciences *102*, 8222-8227.

Nishijima, K., Ng, Y.S., Zhong, L., Bradley, J., Schubert, W., Jo, N., Akita, J., Samuelsson, S.J., Robinson, G.S., Adamis, A.P., and Shima, D.T. (2007). Vascular endothelial growth factor-A is a survival factor for retinal neurons and a critical neuroprotectant during the adaptive response to ischemic injury. The American journal of pathology *171*, 53-67. 10.2353/ajpath.2007.061237.

Nowak, J.Z. (2006). Age-related macular degeneration (AMD): pathogenesis and therapy. Pharmacol Rep *58*, 353-363.

Nozaki, M., Sakurai, E., Raisler, B.J., Baffi, J.Z., Witta, J., Ogura, Y., Brekken, R.A., Sage, E.H., Ambati, B.K., and Ambati, J. (2006). Loss of SPARC-mediated VEGFR-1 suppression after injury reveals a novel antiangiogenic activity of VEGF-A. The Journal of clinical investigation *116*, 422-429. 10.1172/jci26316.

Pallini, R., Pierconti, F., Falchetti, M.L., D'Arcangelo, D., Fernandez, E., Maira, G., D'Ambrosio, E., and Larocca, L.M. (2001a). Evidence for telomerase involvement in the angiogenesis of astrocytic tumors: expression of human telomerase reverse transcriptase messenger RNA by vascular endothelial cells. *94*, 961. 10.3171/jns.2001.94.6.0961.

Pallini, R., Pierconti, F., Falchetti, M.L., D'Arcangelo, D., Fernandez, E., Maira, G., D'Ambrosio, E., and Larocca, L.M. (2001b). Evidence for telomerase involvement in the angiogenesis of astrocytic tumors: expression of human telomerase reverse transcriptase messenger RNA by vascular endothelial cells. J Neurosurg *94*, 961-971. 10.3171/jns.2001.94.6.0961.

Park, J.-I., Venteicher, A.S., Hong, J.Y., Choi, J., Jun, S., Shkreli, M., Chang, W., Meng, Z., Cheung, P., and Ji, H. (2009). Telomerase modulates Wnt signalling by association with target gene chromatin. Nature *460*, 66-72.

Relitti, N., Saraswati, A.P., Federico, S., Khan, T., Brindisi, M., Zisterer, D., Brogi, S., Gemma, S., Butini, S., and Campiani, G. (2020). Telomerase-based Cancer Therapeutics: A Review on their Clinical Trials. Curr Top Med Chem *20*, 433-457. 10.2174/1568026620666200102104930.

Rofagha, S., Bhisitkul, R.B., Boyer, D.S., Sadda, S.R., Zhang, K., and Group, S.-U.S. (2013). Seven-Year Outcomes in Ranibizumab-Treated Patients in ANCHOR, MARINA, and HORIZON: A Multicenter Cohort Study (SEVEN-UP). Ophthalmology. 10.1016/j.ophtha.2013.03.046.

Rossiello, F., Jurk, D., Passos, J.F., and d'Adda di Fagagna, F. (2022). Telomere dysfunction in ageing and age-related diseases. Nat Cell Biol *24*, 135-147. 10.1038/s41556-022-00842-x.

Sakurai, E., Anand, A., Ambati, B.K., van Rooijen, N., and Ambati, J. (2003a). Macrophage depletion inhibits experimental choroidal neovascularization. Invest Ophthalmol Vis Sci *44*, 3578-3585. 10.1167/iovs.03-0097.

Sakurai, E., Anand, A., Ambati, B.K., van Rooijen, N., and Ambati, J. (2003b). Macrophage Depletion Inhibits Experimental Choroidal Neovascularization. Investigative Ophthalmology & Visual Science *44*, 3578-3585. 10.1167/iovs.03-0097.

Sarin, K.Y., Cheung, P., Gilison, D., Lee, E., Tennen, R.I., Wang, E., Artandi, M.K., Oro, A.E., and Artandi, S.E. (2005). Conditional telomerase induction causes proliferation of hair follicle stem cells. Nature *436*, 1048. 10.1038/nature03836

https://www.nature.com/articles/nature03836#supplementary-information.

Shay, J.W., and Bacchetti, S. (1997). A survey of telomerase activity in human cancer. Eur J Cancer *33*, 787-791. 10.1016/S0959-8049(97)00062-2.

Stewart, S.A., Hahn, W.C., O'Connor, B.F., Banner, E.N., Lundberg, A.S., Modha, P., Mizuno, H., Brooks, M.W., Fleming, M., Zimonjic, D.B., et al. (2002). Telomerase contributes to tumorigenesis by a telomere length-independent mechanism. Proc Natl Acad Sci U S A *99*, 12606-12611. 10.1073/pnas.182407599.

Takeda, A., Baffi, J.Z., Kleinman, M.E., Cho, W.G., Nozaki, M., Yamada, K., Kaneko, H., Albuquerque, R.J., Dridi, S., Saito, K., et al. (2009). CCR3 is a target for age-related macular degeneration diagnosis and therapy. Nature *460*, 225-230. 10.1038/nature08151.

Urquidi, V., Tarin, D., and Goodison, S. (2000). Role of telomerase in cell senescence and oncogenesis. Annu Rev Med *51*, 65-79. 10.1146/annurev.med.51.1.65.

Wang, S., Sorenson, C.M., and Sheibani, N. (2012). Lack of Thrombospondin 1 and Exacerbation of Choroidal Neovascularization. Archives of Ophthalmology *130*, 615-620. 10.1001/archopthalmol.2011.1892.

Whikehart, D.R., Register, S.J., Chang, Q., and Montgomery, B. (2000). Relationship of telomeres and p53 in aging bovine corneal endothelial cell cultures. Invest Ophthalmol Vis Sci *41*, 1070-1075.

Yang, J., Chang, E., Cherry, A.M., Bangs, C.D., Oei, Y., Bodnar, A., Bronstein, A., Chiu, C.P., and Herron, G.S. (1999). Human endothelial cell life extension by telomerase expression. J Biol Chem *274*, 26141-26148.

Yang, J., Nagavarapu, U., Relloma, K., Sjaastad, M.D., Moss, W.C., Passaniti, A., and Herron, G.S. (2001). Telomerized human microvasculature is functional in vivo. Nat Biotechnol *19*, 219-224. 10.1038/85655.

Yasuma, R., Cicatiello, V., Mizutani, T., Tudisco, L., Kim, Y., Tarallo, V., Bogdanovich, S., Hirano, Y., Kerur, N., Li, S., et al. (2016). Intravenous immune globulin suppresses angiogenesis in mice and humans. Signal Transduction and Targeted Therapy *1*, 15002. 10.1038/sigtrans.2015.2.

Young, J.I., Sedivy, J.M., and Smith, J.R. (2003). Telomerase expression in normal human fibroblasts stabilizes DNA 5-methylcytosine transferase I. Journal of Biological Chemistry *278*, 19904-19908.

Yu, J., Yuan, X., Sjöholm, L., Liu, T., Kong, F., Ekström, T.J., Björkholm, M., and Xu, D. (2018). Telomerase reverse transcriptase regulates DNMT3B expression/aberrant DNA methylation phenotype and AKT activation in hepatocellular carcinoma. Cancer letters *434*, 33-41.

Zaccagnini, G., Gaetano, C., Della Pietra, L., Nanni, S., Grasselli, A., Mangoni, A., Benvenuto, R., Fabrizi, M., Truffa, S., Germani, A., et al. (2005). Telomerase mediates vascular endothelial growth factor-dependent responsiveness in a rat model of hind limb ischemia. J Biol Chem *280*, 14790-14798. 10.1074/jbc.M414644200.

## HIGHLIGHTS

- Telomerase activity is increased in mouse CNV tissue
- Inhibition of telomerase activity suppresses CNV growth
- Telomerase inhibitor BIBR 1532 and VEGF neutralizing antibodies cooperatively inhibit CNV growth
- The proangiogenic activity of telomerase is independent of its telomere-length maintenance activity
- Telomerase inhibition suppresses induction of angiogenic factors

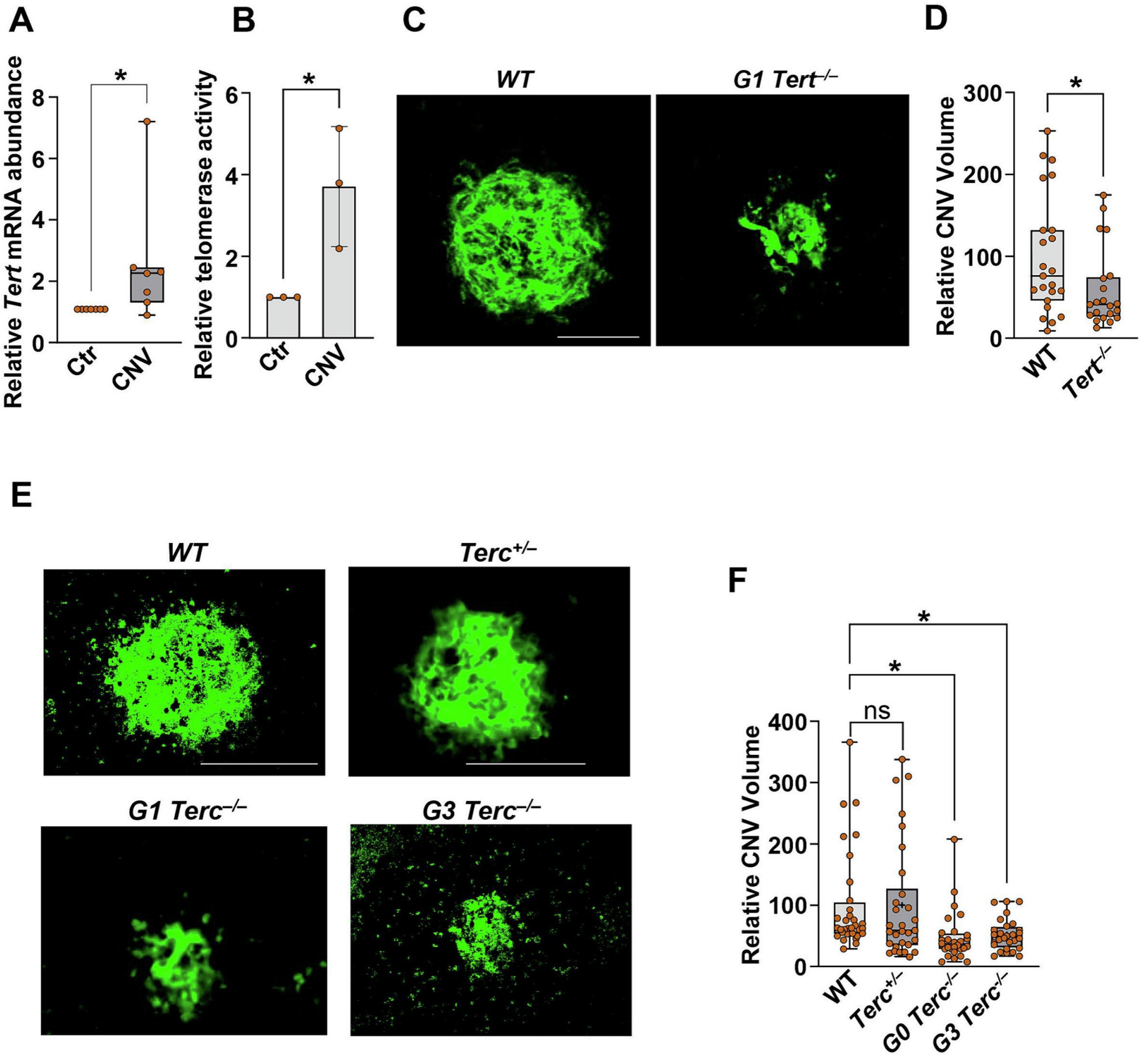
A
Relative Tert mRNA abundance
0
2
4
6
8
*
Ctr
CNV
B
Relative telomerase activity
0
2
4
6
*
Ctr
CNV
C
WT
G1 Tert−/−
D
Relative CNV Volume
0
100
200
300
*
WT
Tert−/−
E
WT
Terc+/−
G1 Terc−/−
G3 Terc−/−
F
Relative CNV Volume
0
100
200
300
400
*
*
ns
WT
Terc+/−
G0 Terc−/−
G3 Terc−/−

Figure 1

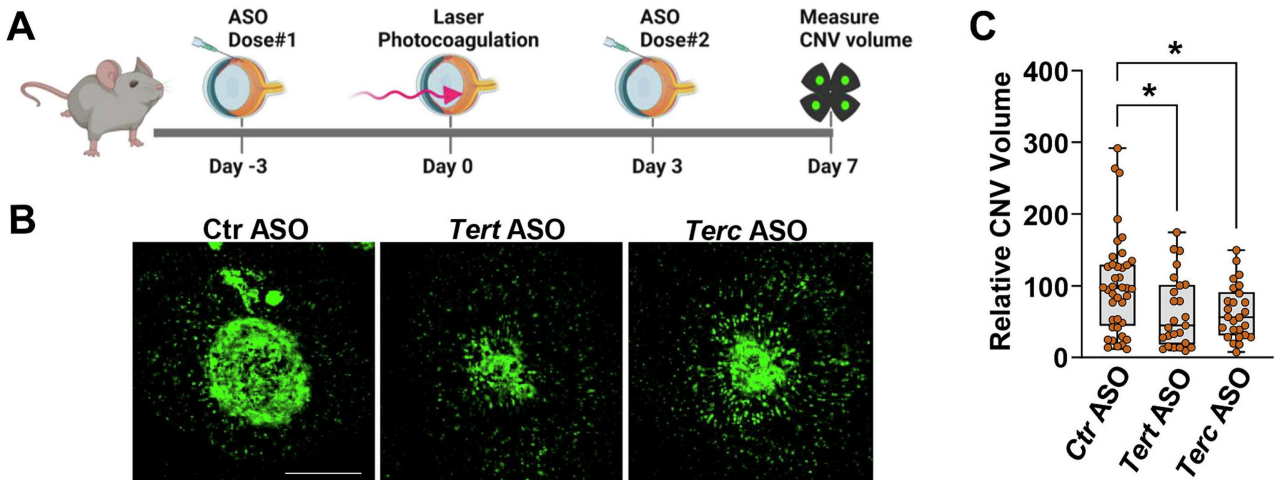
A
ASO
Dose#1
Laser
Photocoagulation
ASO
Dose#2
Measure
CNV volume
Day -3
Day 0
Day 3
Day 7
B
Ctr ASO
Tert ASO
Terc ASO
C
Relative CNV Volume
400
300
200
100
0
*
*
Ctr ASO
Tert ASO
Terc ASO

Figure 2

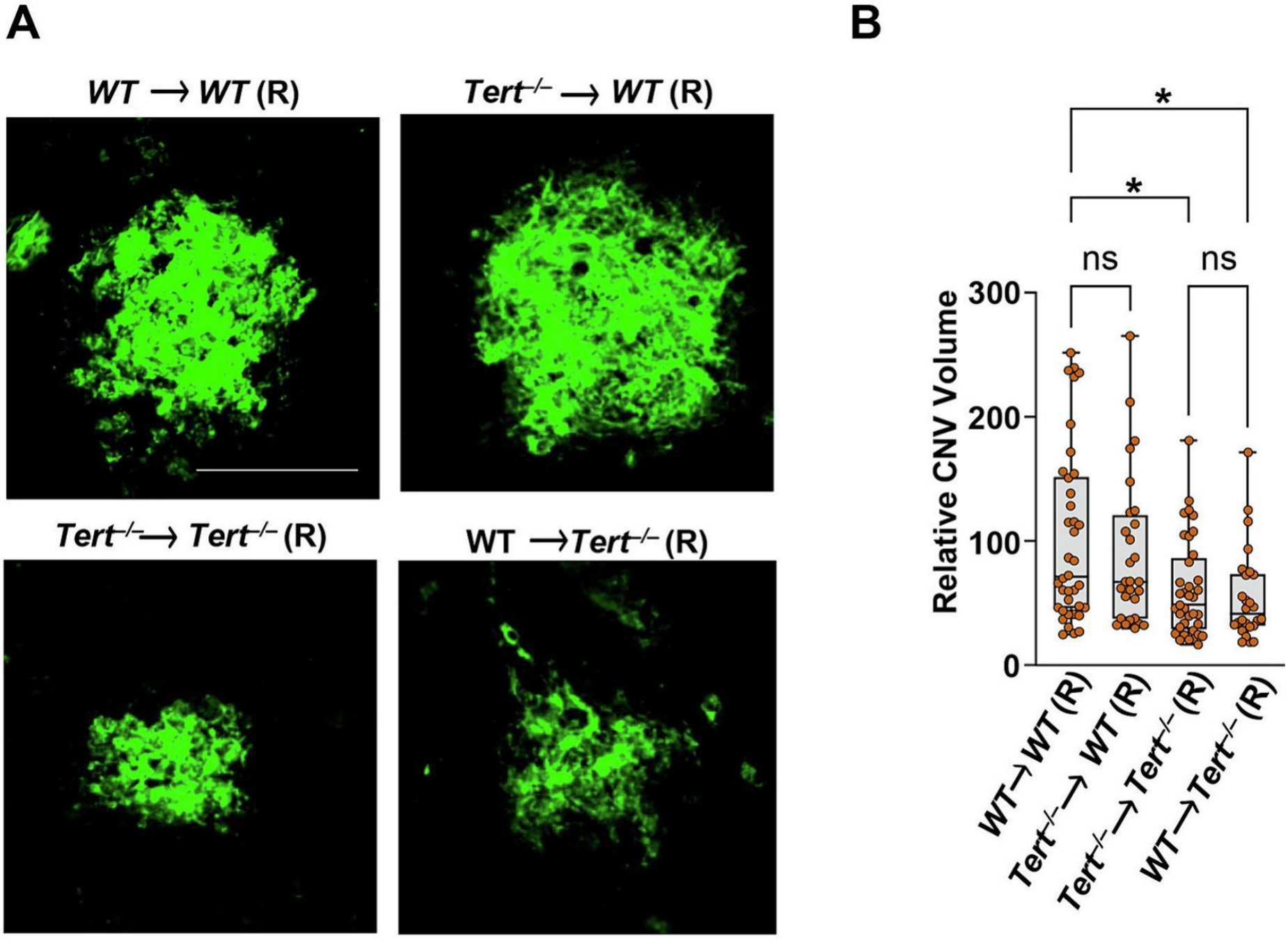
A
WT → WT (R)
Tert-/- → WT (R)
Tert-/- → Tert-/- (R)
WT → Tert-/- (R)
B
*
*
ns
ns
Relative CNV Volume
300
200
100
0
WT→WT (R)
Tert-/- → WT (R)
Tert-/- → Tert-/- (R)
WT→Tert-/- (R)

Figure 3

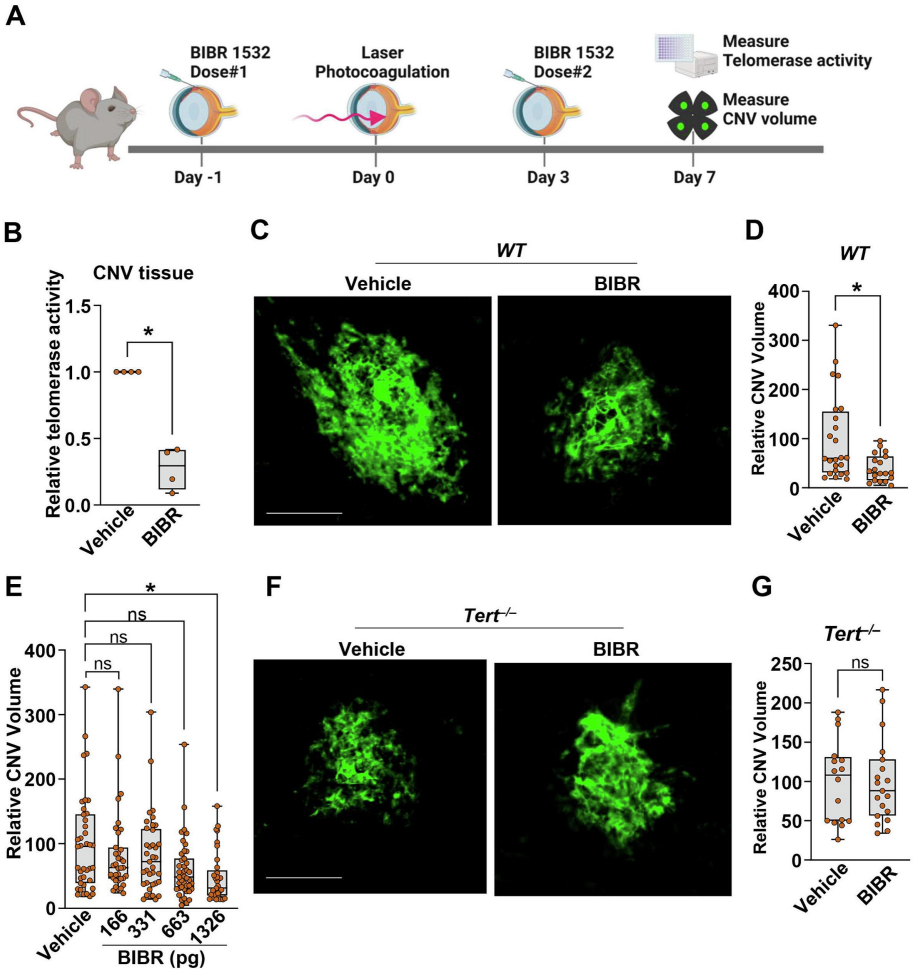
A
BIBR 1532
Dose#1
Laser
Photocoagulation
BIBR 1532
Dose#2
Measure
Telomerase activity
Measure
CNV volume
Day -1
Day 0
Day 3
Day 7
B
CNV tissue
Relative telomerase activity
1.5
1.0
0.5
0.0
*
Vehicle
BIBR
C
WT
Vehicle
BIBR
D
WT
Relative CNV Volume
400
300
200
100
0
*
Vehicle
BIBR
E
*
ns
ns
ns
Relative CNV Volume
400
300
200
100
0
Vehicle
166
331
663
1326
BIBR (pg)
F
Tert−/−
Vehicle
BIBR
G
Tert−/−
Relative CNV Volume
250
200
150
100
50
0
ns
Vehicle
BIBR

Figure 4

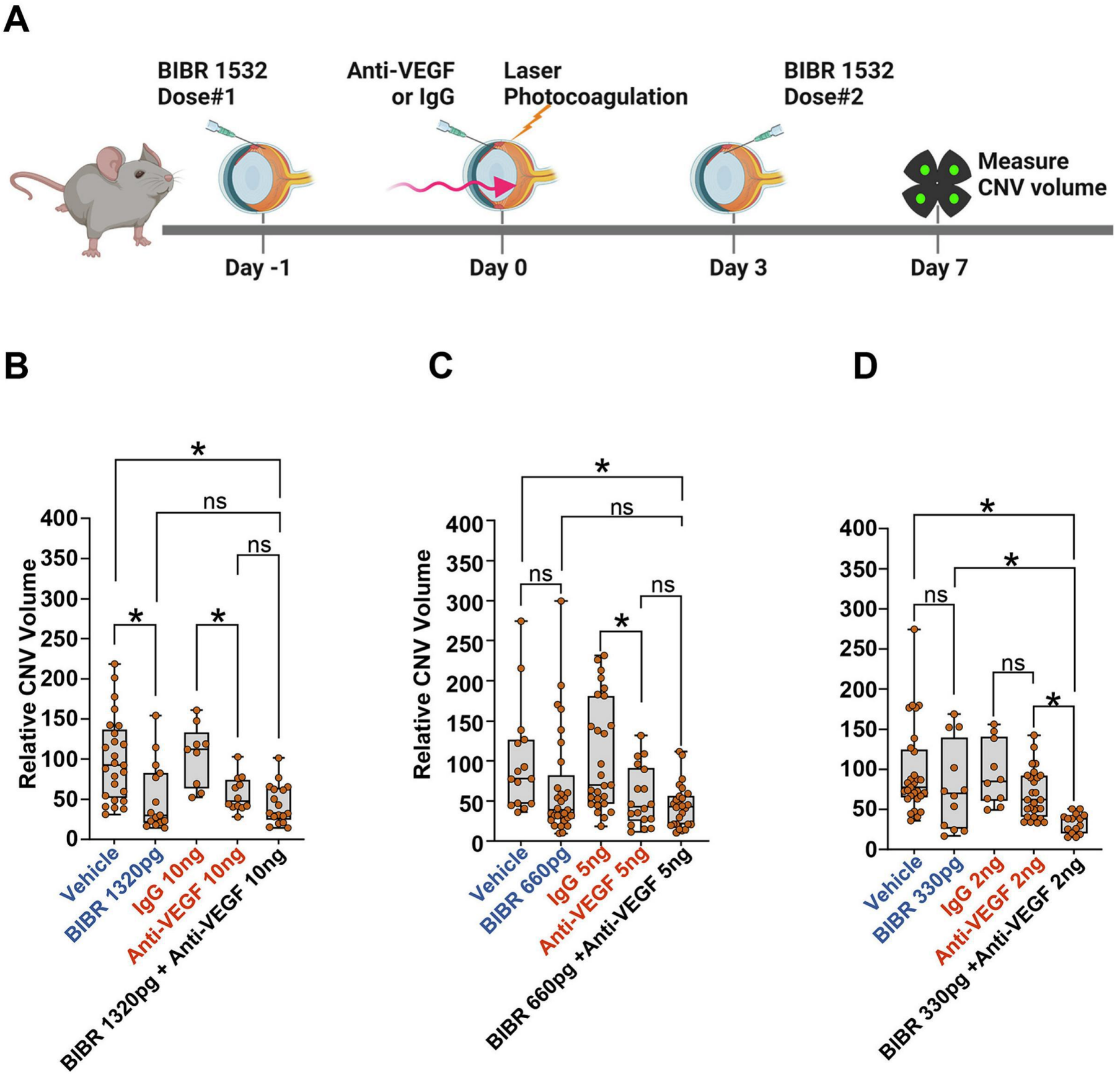
A
BIBR 1532
Dose#1
Anti-VEGF
or IgG
Laser
Photocoagulation
BIBR 1532
Dose#2
Measure
CNV volume
Day -1
Day 0
Day 3
Day 7
B
C
D
Relative CNV Volume
ns
*
Vehicle
BIBR 1320pg
IgG 10ng
Anti-VEGF 10ng
BIBR 1320pg + Anti-VEGF 10ng
BIBR 660pg
IgG 5ng
Anti-VEGF 5ng
BIBR 660pg +Anti-VEGF 5ng
BIBR 330pg
IgG 2ng
Anti-VEGF 2ng
BIBR 330pg +Anti-VEGF 2ng

Figure 5